Known anomalies in 2A12 over land

To improve the current 2A12 rain retrieval algorithm (Kummerow et al. 2001) over land, it is important to evaluate the anomalies in the retrieved product. However, it is difficult to quantify these anomalies globally because there is no single rainfall product that can represent the ground truth. Products from rain gauges have reliable estimation of rainfall *only* over areas with dense rain gauge networks. Rainfall retrieved from the TRMM PR near surface reflectivity has global coverage between 36 N and 36 S, but suffers from uncertain attenuation correction, problems over complex terrain and the limit of minimum detectable signal (Iguchi et al. 2000). In this section, we start the discussion of the anomalies by comparing the rainfall estimates among products from TRMM TMI (2A12), PR (2A25) and rain gauges.

The differences between the 10 year mean 2A12 and 2A25 unconditional monthly rainfall are shown in Figure 1 a-c. Differences between mean 2A12 and unconditional rainfall from rain gauges (GPCC, Rudolf 1995) are shown in Figure 1 d-f. There are both similarities and differences among 2A12, 2A25 and GPCC shown in Figure 1 a-f. They are related to the performance of the algorithms in different weather regimes over different types of land surfaces, and various detection biases.

i.   Biases in strong deep convective systems

The first most obvious anomaly in Figure 1 is the large overestimation of rainfall by 2A12 over central Africa. There is a larger overestimation from 2A12 than 2A25 over GPCC. The sparse rain gauge network over Africa may contribute to uncertainty of GPCC estimates. However, even if GPCC is too low, it is fair to ask why 2A12 has the highest rainfall estimation over central Africa.

To answer this question, TMI defined Precipitation Features (TPFs) are defined by grouping 2A12 raining area using 9 years of TRMM observations (Liu et al. 2008). Then the total volumetric rainfall from 2A12 and 2A25, as well as the maximum height of PR 20 dBZ echo inside each TPF are calculated separately. Then the 2D histograms of the differences between 2A25 and 2A12 volumetric rainfall, and the minimum TMI 85 GHz Polarization Corrected Temperature (PCT, Spencer et al. 1989) in TPFs with size above 2000 km^2 are generated over tropical land and ocean and shown in Figure 2. There are large differences between the histograms over land and over ocean because of the different land and ocean 2A12 algorithms. Over ocean, 2A12 retrieves more rainfall than 2A25 for raining systems with weak convection inferred from relatively high minimum 85 GHz PCT. However, over land, there are two peaks of large overestimation of rain fall by 2A12 over 2A25. One is for systems with weak convection. Another is for systems with strong convection inferred from low minimum 85 GHz PCTs.

It is known that strong deep convection lifts large amounts of ice to high altitudes, causing strong scattering of the upwelling radiance from below by the ice hydrometeors, leading to depression of the brightness temperature at 85 GHz. Because the 2A12 land

algorithm depends so strongly upon this ice scattering signal, the algorithm derives high rainfall rates for these cases. However, the strong attenuation of radar reflectivities caused by the large amount of ice in these cases may lead to underestimation of rainfall by 2A25. Central Africa is known to have the strongest convective systems anywhere in the tropics (Liu and Zipser, 2005). Therefore, we speculate that the overestimation of 2A12 over 2A25 and GPCC is caused by different errors of estimation of rainfall rates in the strong convective systems over the region. This may also explain the overestimation of rainfall by 2A12 over regions known for their strong convection (Zipser et al. 2006), such as the Southern plains of the US in JJA (Figure 1b and 1e), and Argentina in DJF (Figure 1c 1f).

ii.   Underestimation of warm rainfall

It is obvious that a retrieval algorithm mainly relying on the ice scattering would have trouble detecting warm rainfall. From Liu and Zipser (2008), there is a large amount of trade wind warm rainfall over the east coast of Brazil, Madagascar, Philippines, and Costa Rica in winter and west coast of India in summer. It is consistent that 2A12 shows less unconditional rainfall than 2A25 over the corresponding regions in those seasons in Figure 1b and 1c. It is very likely that the TRMM PR as well may underestimate the warm rainfall over these regions due to the limit of the minimum detectable reflectivity around 17 dBZ. Therefore, the underestimation of the 2A12 rainfall over these regions during the warm rain season is more obvious by comparing with GPCC (Figure 1e and 1f).

iii.   "False alarm" over arid land and snow surface

Properly identifying raining area from surface areas that produce a microwave signature similar to that of precipitation has always been a challenge (Grody 1991, Ferraro et al. 1998). There are two types of surface areas that are extremely difficult to identify: arid desert and snow. As shown in Figure 3, the current 2A12 land algorithm (Ferraro et al. 1998) detects much more unrealistic raining area than 2A25 over the Sahara (Figure 3b) and Kalahari (Figure 3c) deserts in Africa during the dry seasons. It also detects large unrealistic raining areas over snow covered high terrain, including Tibet, Iran, and the Rocky Mountains during boreal winter and over the Andes and Altiplano during austral winter. These over-detection anomalies can explain the overestimation of rainfall by the 2A12 land algorithm over these regions in Figure 1.

iv.   Other anomalies

An advantage of using a screening algorithm is to remove the false alarm of precipitation over a snow covered surface. However, this also prevents the detection of actual precipitation in the form of snow. For example, in Figure 4, there are clear ice scattering signals with brightness temperature depressions at 85 GHz (Figure 4a) due to precipitation in the form of snow occupying a fairly deep layer. However, these signals are not recognized as precipitation because of the screening algorithm in 2A12, so that 2A12 retrieves nearly no precipitation for this snow case.

Some differences between 2A12 to 2A25 are due to differing horizontal resolution. As shown in Figure 5, the fine structure of convection shown by PR over New Mexico, US is smeared by 2A12 due to using the information of the TMI low frequency channels with relatively larger footprints (Kummerow et al. 1998).

Thick anvil clouds may be related to another possible anomaly in 2A12 because they can lead to enough ice scattering signals to satisfy the precipitation criteria in 2A12 over land. There are cases found with large areas of thick anvil for which the 2A25 algorithm shows no surface rainfall because there is no detectable radar echo reaching near the ground. However, 2A12 sometimes reports large areas of rainfall under these thick anvil clouds (not shown). These cases may partially explain the higher rain detection by 2A12 than 2A25 over central Africa (Figure 3a-c), Argentina in DJF (Figure 3b) and the southern plains of the US in JJA (Figure 3c.

In this section, we have listed a few scenarios that may explain some of the important differences among 2A12, 2A25 and GPCC rainfall products. However, there are still questions to be answered. For example, why do both 2A12 and 2A25 report lower rainfall than GPCC over Bay of Bengal, Southeast China and southern Nigeria in JJA, and near the mouth of the Amazon in DJF? Is this from the underestimation by both algorithms for systems dominated by relatively shallow, mostly warm rain? What kind of weak precipitation systems lead to higher/lower 2A12 rainfall than 2A25 as shown in Figure 2? Further investigations on these are warranted.

References

Ferraro, R. R., E. A. Smith, W. Berg, and G. J. Huffman, A screening methodology for passive microwave precipitation retrieval algorithms, *J. Atmos. Sci.*, **55**, 1583-1600, 1998.

Grody, N. C., Classification of snow cover and precipitation using the Special Sensor Microwave Imager, *J . Geophys. Res.*, **96**, 7423-7435, 1991.

Iguchi, T., T. Kozu., R. Meneghini, J. Awaka, and K. Okamoto, Rain-profiling algorithm for the TRMM precipitation radar. *J. Appl. Meteor.*, **39**, 2038-2052, 2000.

Kummerow, C., W. Barnes, T. Kozu, J. Shiue, and Joanne Simpson, The Tropical Rainfall Measuring Mission (TRMM) Sensor Package. *J. Atmos. Oceanic Tech.,* **15**, 809–817, 1998.

Kummerow, C., Y. Hong, W. S. Olson, S. Yang, R. F. Adler, J. McCollum, R. Ferraro, G. Petty, D.-B. Shin, and T. T. Wilheit. The Evolution of the Goddard Profiling Algorithm (GPROF) for rainfall estimation from passive microwave sensors. *J. Appl. Meteor.,* **40**, 1801–1820, 2001.

Liu, C., and E. J. Zipser, "Warm rain" in the tropics: Seasonal and regional distribution based on 9 years of TRMM data, *J. Climate*, submitted, 2008.

Liu, C., E. J. Zipser, D. Cecil, S. W. Nesbitt, and S. Sherwood, A cloud and precipitation feature database from 9 years of TRMM observations, *J. Appl. Meteor. Climatol*, in press, DOI:10.1175/2008JAMC1890.1, 2008.

Liu, C., and E. J. Zipser, Global distribution of convection penetrating the tropical tropopause, *J. Geophys. Res.*, doi:10.1029/2005JD00006063, 2005.

Rudolf, B., Global Precipitation Climatology Centre. In: WMO/UNEP, The global climate system review, climate system monitoring June 1991 - November 1993. *WMO-No. 819, Genf*, 37, 1995.

Spencer, R. W., H. G. Goodman, and R. E. Hood, Precipitation retrieval over land and ocean with the SSM/I: identification and characteristics of the scattering signal. *J. Atmos. Oceanic Tech.*, **6**, 254-273, 1989.

Zipser, E., D. Cecil, C. Liu, S. W. Nesbitt, and S. Yorty, where are the most intense thunderstorms on Earth?, *Bull. Am. Meteorol. Res*.,**87**, 1057-1071, 2006.
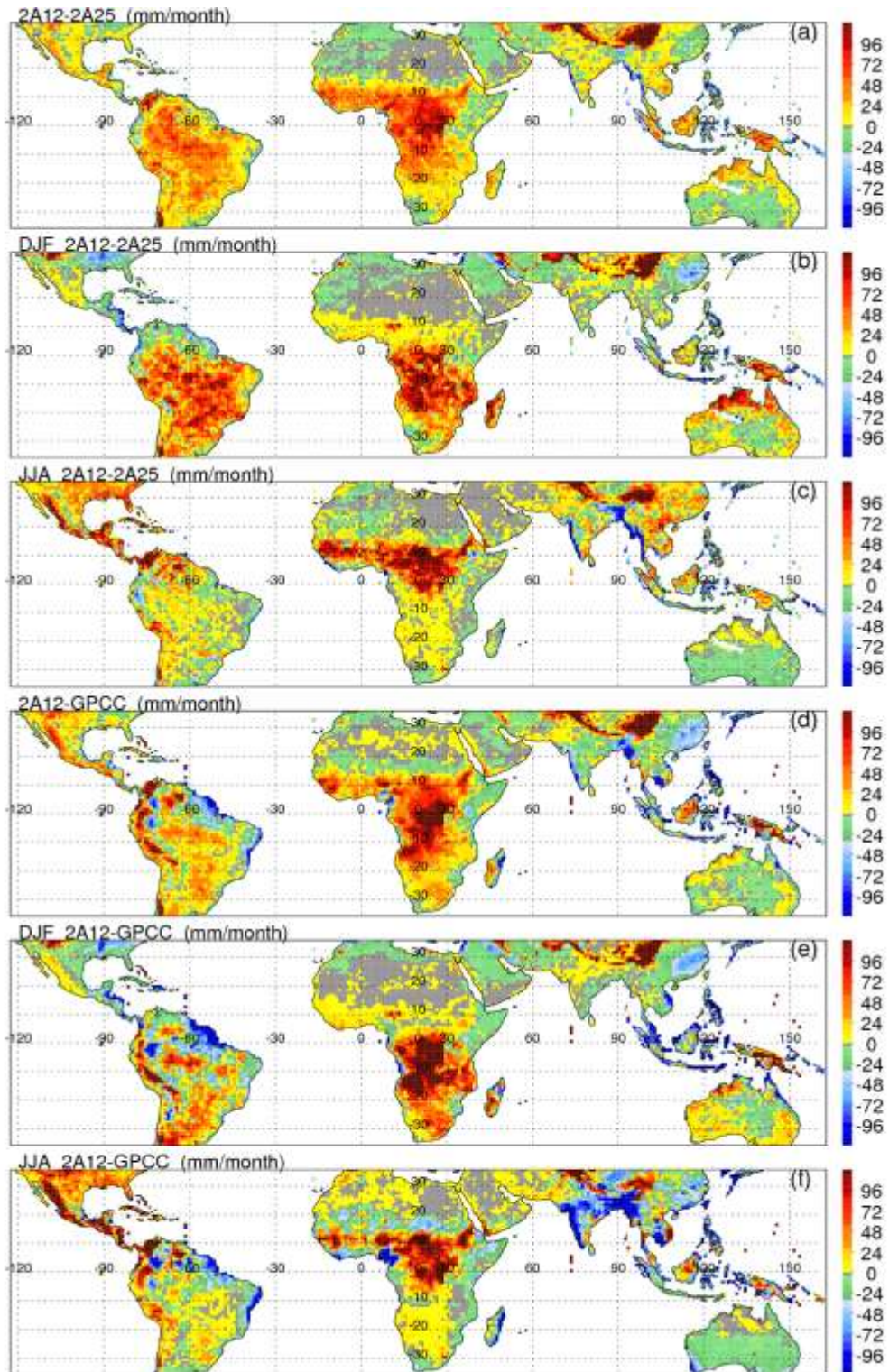
Figure 1. Differences among 10 year mean unconditional monthly rainfall from TRMM PR, TMI and rain gauges (GPCC).
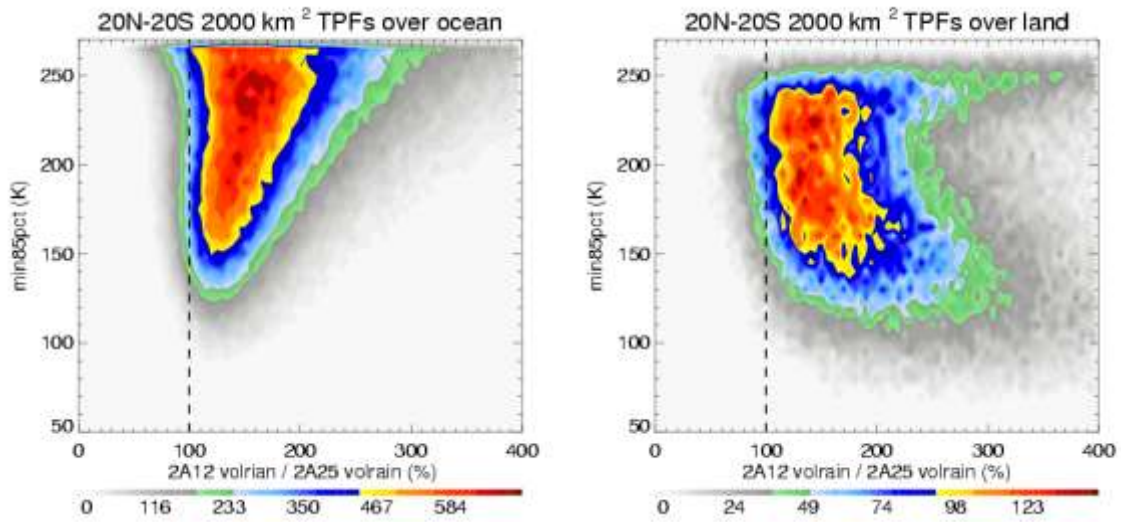
.

Figure 2. 2D histogram of rainfall differences from 2A12 and 2A25 and minimum 85 GHz PCT in the precipitation features defined by 2A12 raining area with size greater than 2000 km^2 over tropical land and ocean.
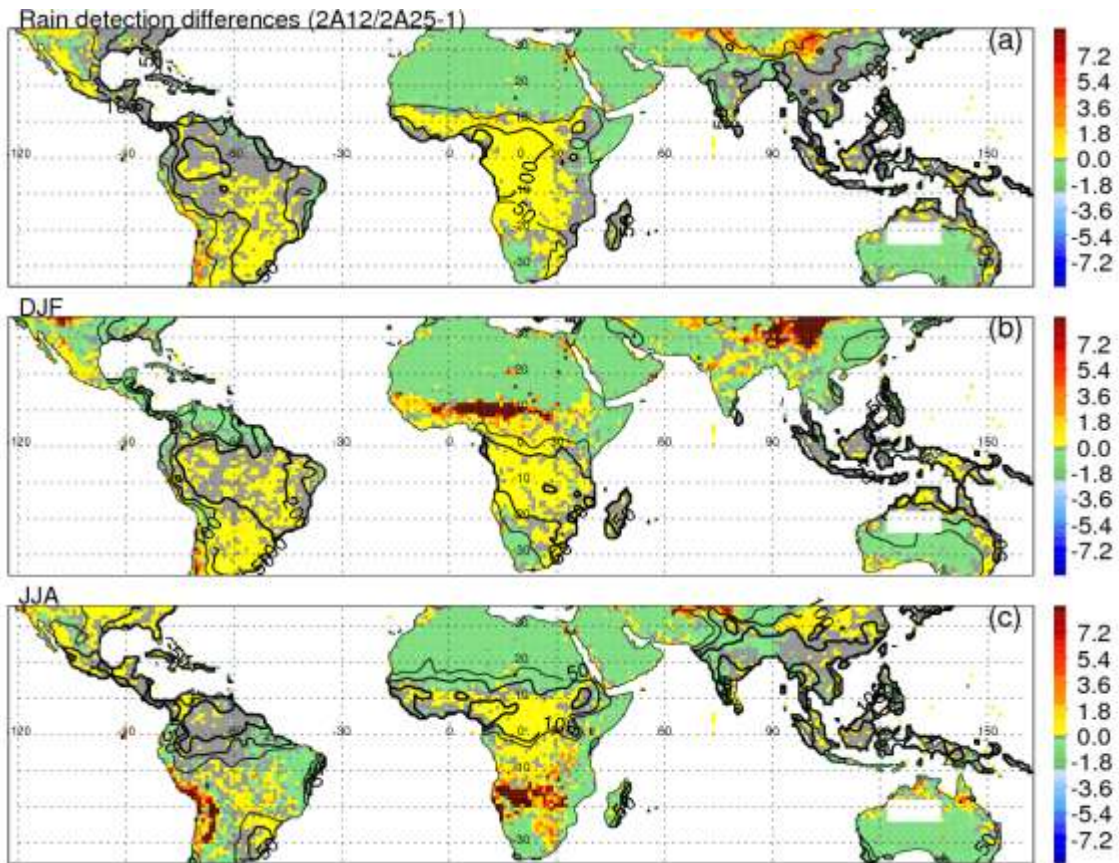
Figure 3. Rain detection differences (color fill) between TRMM 2A25 and TRMM 2A12 in ratios. The GPCC unconditional rainfall (units are in mm/month) is shown in contours. Note that there is a large area over North Australia missing due to lack of observations by the TRMM PR.
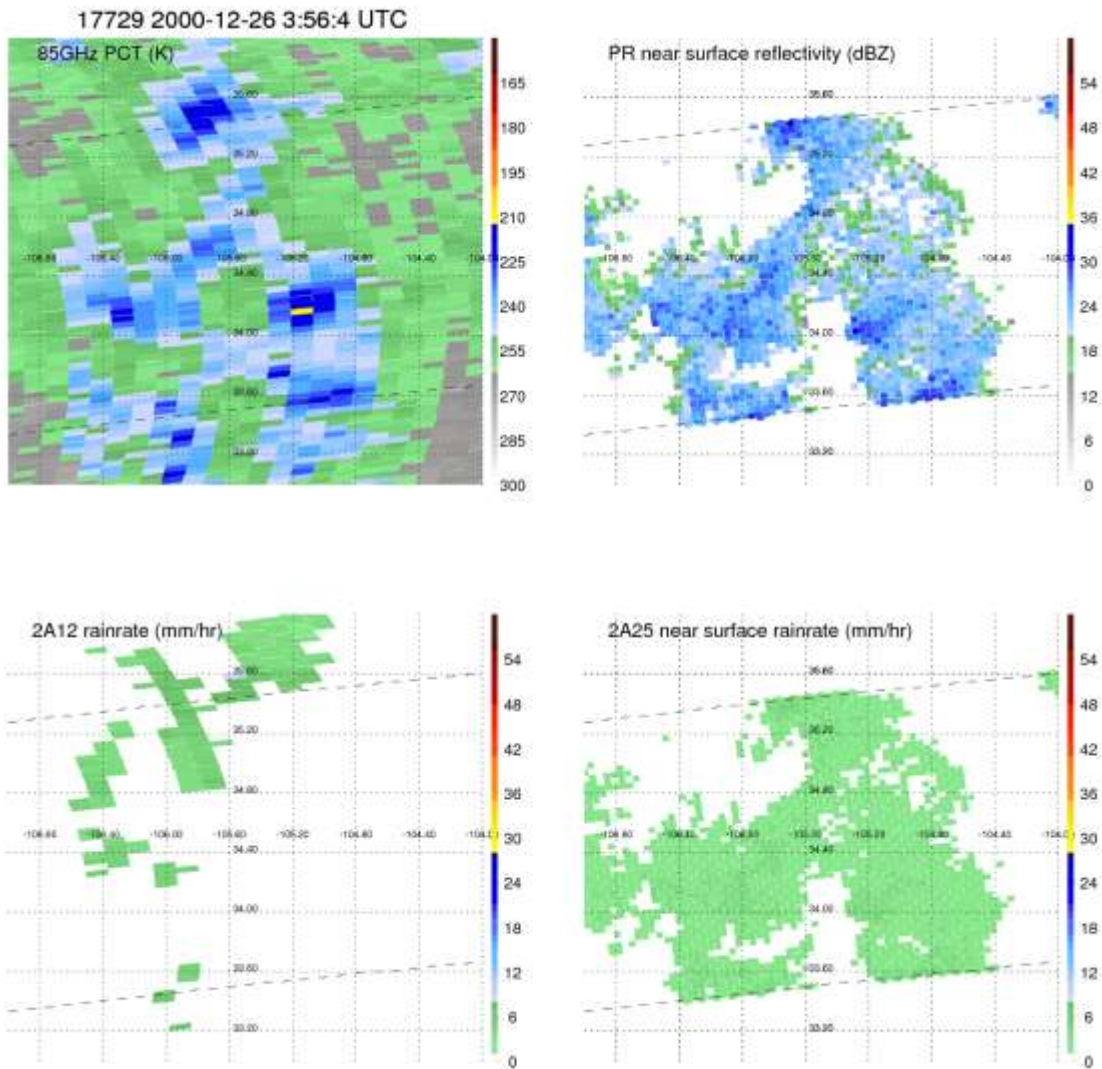
Figure 4. A snow case over New Mexico on December 26, 2000. The NCEP surface temperature was near 269 K over the region. The ice scattering signature at 85 GHz from precipitation in top left panel is consistent with the near surface reflectivity pattern from the PR in the top right panel. However, 2A12 (bottom left) missed most of the region of precipitation for this case.
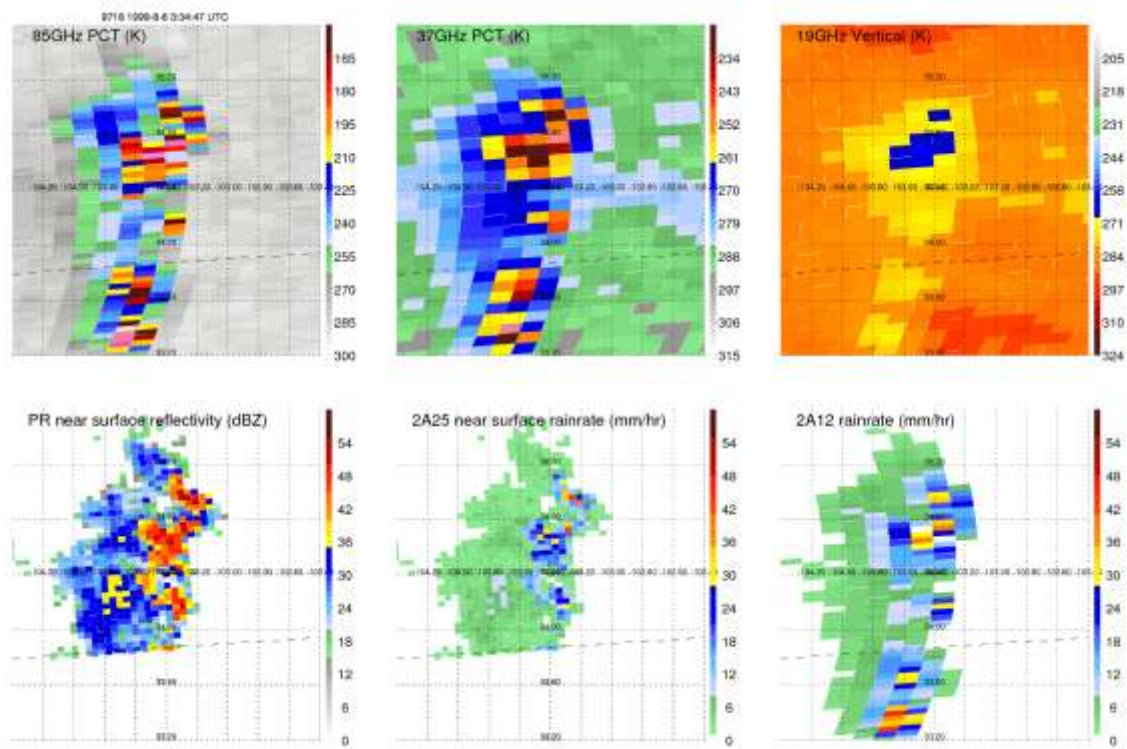
Figure 5. A line of convection over New Mexico on August 6, 1999. The TRMM PR shows a typical structure of a leading convective line and the trailing stratiform in bottom left panel. This fine scale structure could not be captured by the TMI due to the larger footprints of TMI. This leads to a relatively larger area with moderate rainfall rate in 2A12 retrievals (bottom right panel) compared to the heavy rainfall rate in the convective region and lower rainfall rate in the stratiform region shown by 2A25 (bottom middle panel).